In-plane *I-V* characteristics of interlayer Josephson vortices in cuprate high-T_c superconductors: Dynamical simulations

Qing-Hu Chen[1,2] and Xiao Hu[1]
[1]*Computational Materials Science Center, National Institute for Materials Science, Tsukuba 305-0047, Japan*
[2]*Department of Physics, Zhejiang University, Hangzhou 310027, People's Republic of China*
(Received 14 November 2006; published 13 February 2007)

Computer simulations on Josephson vortex systems driven by in-plane currents in cuprate high-T_c superconductors have been performed. For high anisotropy and magnetic field, we find power-law *I-V* characteristics with the index jumping from 1 (i.e., Ohmic) at high temperatures to $\geqslant 3$ (i.e., non-Ohmic) at intermediate temperatures, which can be attributed to a Kosterlitz-Thouless (KT) transition. In the KT phase, simulations reveal a resistivity independent of the angle between the current and the magnetic field, i.e., *orientation-independent dissipation*, due to the intralayer quasi-long-range order and interlayer short-range order of Josephson vortices. For low anisotropy and magnetic field, an orientation-dependent non-Ohmic dissipation is observed where the three-dimensional long-range order exists. The present approach provides a unified explanation to previous experimental observations in the non-Ohmic regime.

DOI: 10.1103/PhysRevB.75.064504 PACS number(s): 74.72.−h, 74.25.Qt, 74.40.+k

I. INTRODUCTION

The cuprate high-T_c superconductors are layered compounds where the superconductivity occurs mainly in the CuO planes separated by block layers. The effect of the layered structure on the in-plane resistivity is a long-standing issue,[1] and still not fully understood. When a magnetic field is applied parallel to the CuO plane, Josephson vortices (JVs) are induced and are located at the block layers. The CuO planes play pronounced intrinsic pinning effects on the movement of JV in the vertical direction. An intriguing transport phenomenon has been found in strong layering Bi- and Tl-based materials by Iye *et al.*[2] and Woo *et al.*[3] that the resistivity in the non-Ohmic regime does not depend on the angle between the magnetic field and current when they are both parallel to the layers. Power-law, non-Ohmic dissipations have been observed in $Bi_2Sr_2CaCu_2O_{8+y}$ by Ando *et al.*[4] and Pradhan *et al.*[5] On the other hand, an orientation dependent non-Ohmic dissipation was observed in weak layering $YBa_2Cu_3O_{7-\delta}$ single crystal by Kwok *et al.*[6] It is worthwhile to note that the experimental investigation for JV systems relies heavily on transport measurements because their large cores make Bitter decorating and magneto-optical techniques more difficult than for pancake vortices (PVs) in CuO planes.

Chakravarty *et al.* pointed out that the orientation-independent non-Ohmic dissipation cannot occur in a lattice phase.[7] Blatter *et al.*[8] proposed a novel Kosterlitz-Thouless (KT) (Refs. 9 and 10) scenario at high magnetic fields, characterizing the behavior by a state with vanishing interlayer shear modulus. Recently, Hu and Tachiki[11] found by equilibrium computer simulations a novel KT phase, characterized by the interlayer short-range (SR) and intralayer quasi-long-range order (QLRO) of JVs, in intermediate temperature regime for high anisotropy parameter and magnetic field. For low anisotropy parameters similar to that of $YBa_2Cu_3O_{7-\delta}$ investigated in Ref. 6, it is difficult to achieve the above situation since the required magnetic field is above $B_{mc} \simeq \phi_0/2\gamma d^2 \sim 150$ T.[8,11–13] In the latter case, the non-Ohmic dissipation occurs in the lattice phase of three-dimensional (3D) LRO.

The above-mentioned novel KT phase seems to be one of the manifestations of the *sliding phase* in layered systems.[14] The hallmark Hamiltonian of the sliding phase is a stack of otherwise independent 2D elastic Hamiltonians with interlayer couplings between in-plane phase gradients.[15] The stability of the sliding phase is displayed by tuning the interlayer gradient couplings such that Josephson-like interlayer couplings become irrelevant at a lower temperature than the KT transition point where intralayer QLROs are destroyed.[15] The sliding phase is enhanced by an in-plane magnetic field.[16] It is worthy to notice that to add a constant phase on a given CuO layer corresponds to drive JVs in the two sandwiching block layers in opposite directions. It is not difficult to see that in large magnetic field where a dense triangular JV lattice is realized at low temperatures, thermal fluctuations induce interlayer couplings between supercurrents predominantly in the same way that the sliding phase is stabilized, revealed in Ref. 15.

In order to build a bridge between the equilibrium phases and the transport properties, which have been accessed in many experiments, we perform large-scale dynamical simulation in the present study. The remaining part of the paper is organized as follows. In Sec. II, the Hamiltonian and the dynamic equations are introduced, along with a description of the numerical algorithm for simulation. Section III contains simulation results and discussions, and a brief summary is presented in the last section.

II. MODEL

The Hamiltonian is for the phases of the superconductivity order parameter on the simple cubic grid,[17,18]

$$\mathcal{H} = -J \sum_{\langle i,j\rangle \| x,y \text{ axis}} \cos(\varphi_i - \varphi_j) - \frac{J}{\gamma^2} \sum_{\langle i,j\rangle \| c \text{ axis}} \cos\left(\varphi_i - \varphi_j - \frac{2\pi}{\phi_0}\int_i^j A_c dr_c\right), \quad (1)$$

where $J=\phi_0^2 d/16\pi^3\lambda_{ab}^2$, the y direction is along the external magnetic field and $\hat{x}\perp\hat{c}\perp\hat{y}$, $\mathbf{A}=(0,0,-xB)$, and $\gamma=\lambda_c/\lambda_{ab}$. The system is of size $L_x\times L_y\times L_c=256d\times 256d\times 20d$ under periodic boundary conditions, with d the separation between CuO layers. We fix the density of JV lines at $f=Bd^2/\phi_0=1/32$ and take two typical anisotropy parameters $\gamma=8$ and $\gamma=20$,[11] which correspond to systems below and above the multicritical point, respectively.

The resistivity-shunted-junction (RSJ) dynamics is incorporated in simulations, which can be described as[19,20]

$$\frac{\sigma\hbar}{2e}\sum_j(\dot{\phi}_i-\dot{\phi}_j) = -\frac{\partial H}{\partial\phi_i} + J_{\text{ext},i} - \sum_j \eta_{ij}, \quad (2)$$

for the ith site where $J_{\text{ext},i}$ is the in-plane external current and is zero except for the boundary sites. η_{ij} is the thermal noise current with zero mean and a correlator $\langle\eta_{ij}(t)\eta_{ij}(t')\rangle=2\sigma k_B T\delta(t-t')$. In the following, the units are taken of $2e=J_0=\hbar=\sigma=k_B=1$. In the present simulation, the fluctuating twist boundary condition[19] is applied in the xy plane to maintain the current, and the periodic boundary condition is employed in the c axis. Details on the simulation technique of RSJ dynamics can be found in Ref. 18.

The main results for the equilibrium state by Monte Carlo simulations[11] are reproduced by the present RSJ simulations putting the external current to zero. In the calculated structure factor, δ function Bragg peaks at the reciprocal-lattice vectors are clearly found below the melting temperature $T_m\simeq 0.96$ for $\gamma=8$ while they disappear for $\gamma=20$ even below the superconductivity transition point roughly equal to T_m numerically. Our dynamical simulations are started from initial phase configurations in equilibrium state, and external currents are added gradually. Our runs are typically of $(2\sim 4)\times 10^7$ time steps and the latter half time steps are used for measurements. We calculate the voltage drop along the current direction.[18]

III. RESULTS AND DISCUSSIONS

In order to elucidate the effect of the Lorentz force on the transport properties, the external current is applied either parallel or perpendicular to the magnetic field. The current dependence of voltage below the equilibrium transition temperature[11] is plotted in Fig. 1(a) for $\gamma=20$. Error bars are smaller than the symbol sizes. It is intriguing to observe that below the transition temperature, the current-voltage characteristics are independent of the current direction. We have also simulated the I-V characteristics for current in other intermediate directions, and could not find any voltage deviation. This result agrees well with previous experimental observations conducted in highly anisotropic materials under sufficiently strong magnetic fields.[2,3]

The I-V curves for $\gamma=20$ show nice power-law behaviors with index $\alpha=3.38$ and $\alpha=4.44$ for $T=0.8$ and $T=0.9$, respectively, similar to the KT ones originally observed in pure 2D systems.[21] This observation is consistent with the results of MC simulations,[11] where c-axis SR correlations of JV lines are revealed and thus the system is essentially of 2D nature. In order to study the KT dynamics in more detail, we have calculated the resistivity $R=V/I$ as a function of current I around the KT transition point. As presented in Fig. 2, $R=V/I$ tends to a finite value as the current decreases at high temperatures, corresponding to an Ohmic resistivity. It should be noticed that for high temperatures even smaller currents are necessary in order to achieve the true Ohmic situation, which, however, demands huge systems for simulation. On the other hand, power-law curves appear at low temperatures. This is just the celebratory dynamical behavior of the KT state. A curve with slope equal to 2 is just in between these two groups of curves, demonstrating that the I-V index jumps from 3 to 1 at the KT transition temperature. From the present data we estimate $T_{\text{KT}}\simeq 0.93$ which is slightly below that of equilibrium simulations.[11] The discrepancy may be due to different size dependences of measured quantities.

In Fig. 1(b), we present voltage against current for currents both parallel and perpendicular to the magnetic field for

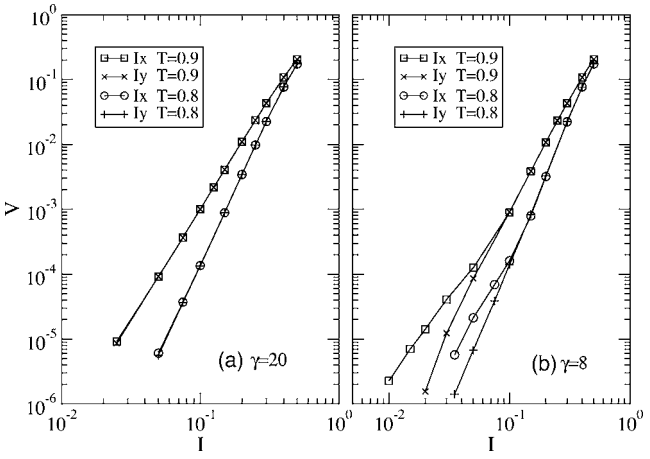

FIG. 1. Current dependence of voltage for currents parallel (I_y) and perpendicular (I_x) to the magnetic field at temperatures $T=0.8$ and 0.9 for (a) $\gamma=20$ and (b) $\gamma=8$. The vortex density is fixed at $f=1/32$. The lines are merely a guide for the eye.

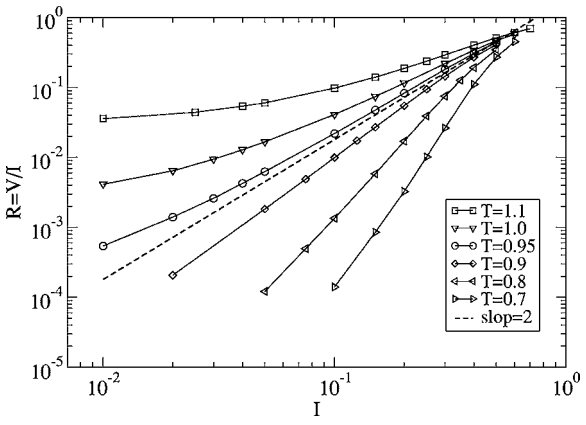

FIG. 2. Current dependence of resistivity for $\gamma=20$ at various temperatures.

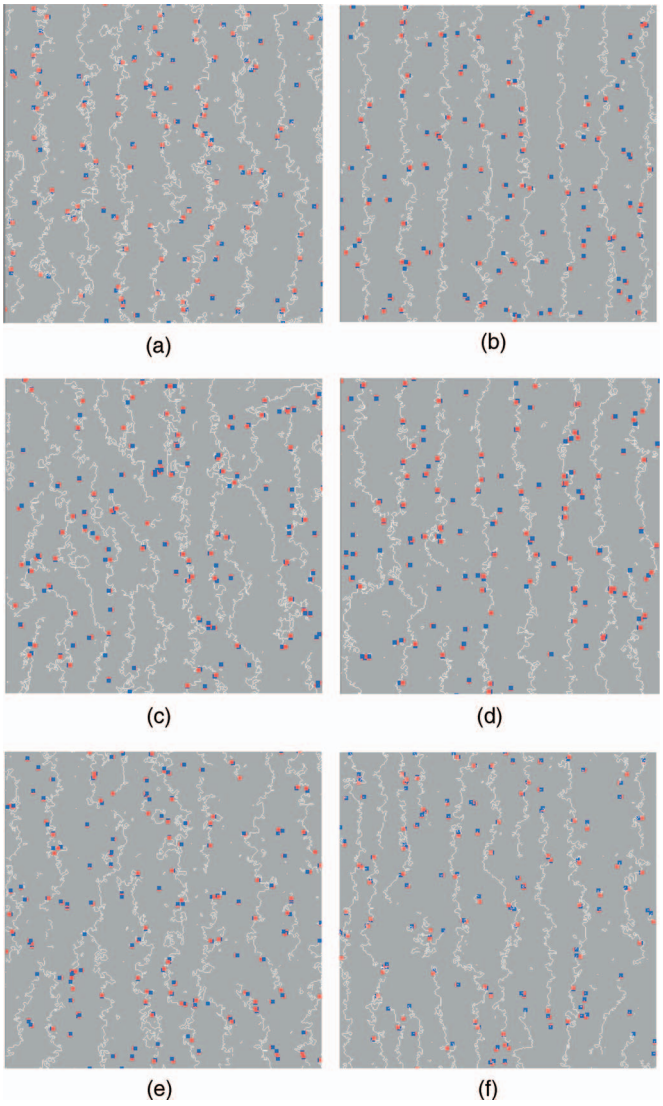

FIG. 3. (Color) Real-space configurations of JV lines in a certain block layer and PV on the CuO plane above for $\gamma=20$ with currents $I=0$ and $I=0.025$ (left column) and $\gamma=8$ with currents $I=0$ and $I=0.02$ (right column) at $T=0.9$. Top, middle, and bottom rows are for equilibrium, $I\|B$ and $I\perp B$, respectively.

$\gamma=8$ at $T=0.8$ and $T=0.9$, which are below the first-order melting transition temperature where 3D LRO is observed in equilibrium.[11] Interestingly, we find that the in-plane resistivity is orientation dependent for currents small enough. The excess voltage for $I\perp B$ over $I\|B$ agrees with the previous experimental results observed in weakly anisotropic layering Y-Ba-Cu-O (YBCO) single crystal under relatively weak magnetic fields.[6]

In order to clarify the mechanism of the above observations on a *microscopic* level, we investigate the real-space configurations of vortices. At finite temperature and applied current, JV lines meander and creep into neighboring block layers by creating pairs of pancake vortex and antivortex in CuO planes. The JV lines in one block layer and the PVs in the CuO layer above are visualized in Fig. 3 for equilibrium state and the simulated lowest currents of two typical directions. To describe the intralayer JV correlations, we also present the corresponding partial structure factor $S(k_x,k_y)\equiv\frac{1}{L_z}\Sigma_z S(k_x,k_y,z)$ in Fig. 4.

For $\gamma=20$ and $T=0.9$, JV lines meander even in large length scale as shown clearly in the top-left panel of Fig. 3, which corresponds to the in-plane QLRO in the KT phase. We have observed that many PV pairs with small separations are generated along the JV lines, indicating that hops of small JV segments are predominant in equilibrium. When an in-plane current is applied, due to the zigzag configurations of JV lines, Lorentz force equal for the two directions of current pushes JV segments up. Due to the intrinsic pinning, this motion proceeds via a nucleation process. A nucleus is bounded by two PVs. We find that the separations of these PV pairs, which are nothing but sizes of dislocations in JV alignment, are larger than those of thermally excited ones. The voltage bias at low in-plane currents is dominated by unbinding of these large-sized PV pairs inside the superconducting layers, which will be calculated in the following. The interlayer SR of the JV is equivalent to the vanishing interlayer shear modulus conjectured in the previous theory.[8] Although a computer simulation cannot analytically give the energy in creating PVs, we argue that the intralayer QLRO of JVs results in logarithmic dependence of activation energy on the current density, which in turn produce the KT dynamics in the present system.

For $\gamma=8$ and $T=0.9$, JV lines are straight in large scale as shown in the top-right panel of Fig. 3. When current is applied along the field, the JV lines do not feel Lorentz force very much, and thus the LRO remains almost unchanged. The voltage is generated mainly due to the unbinding of thermally activated PV pairs. We believe that this is the origin of the background voltage observed experimentally in $I\|B$.[6] When current is perpendicular to the field, the Lorentz force becomes maximal, which facilitates significantly hops of JV segments across CuO layers into neighboring block layers, by creating PV pairs with large separations. Hops of JV segments disturb intralayer correlations and weaken the interlayer correlations as well. In this way, the JV system becomes more disordered even than the JV system of $\gamma=20$ driven by a slightly higher current as shown in the bottom panels of Figs. 3 and 4.

Finally, we quantitatively study the number of PVs and relate the observed voltage to motion of vortices transverse to the current. For RSJ dynamics, we have (see, e.g., Ref. 22) $V\propto N_+\bar{v}_+-N_-\bar{v}_-$. Here $N_\pm$ are the numbers of $\pm$ vortices in the system, and $\bar{v}_\pm$ are their mean velocities in the transverse direction. Note that correlated drift of a vortex-antivortex pair does not contribute to voltage. For layered superconductors with in-plane current only PVs contribute to the macroscopic voltage. At weak currents, the mean drift velocity $\bar{v}_+=-\bar{v}_-$ is proportional to I, so the voltage is roughly decided by the number of free PVs. Two PVs are considered as free when they are dissociated such that the size of the vortex pair is larger than the vortex-antivortex pair breaking scale $l_b\sim I^{-1}$, by overcoming the maximal activation energy.[20,21]

Figure 5 illustrates the number of PV "pairs" after eliminating vortex-antivortex pairs of small sizes through a coarse-graining procedure at $T=0.9$ for equilibrium state and the lowest accessible currents. We present the numerical re-

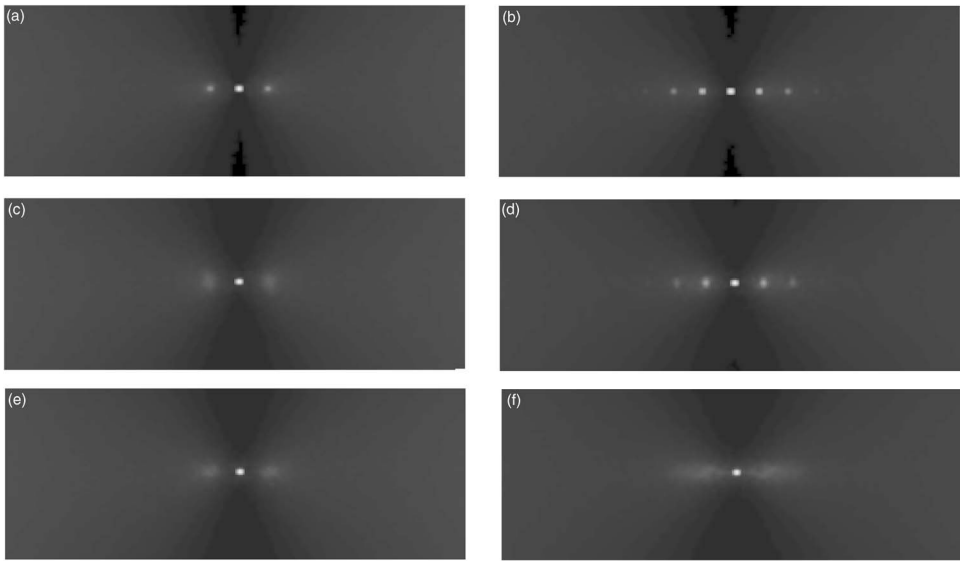

FIG. 4. Partial vortex structure factors $S(k_x,k_y)$ corresponding to those shown in Fig. 3.

sults in this way since it is usually hard to figure out l_b explicitly. For $\gamma=20$, it is clear that within statistical errors the number of PV pairs with sizes larger than any given length is the same for currents perpendicular and parallel to the magnetic field. This results in the equal voltage drops for the two current directions. For $\gamma=8$, the number of PV pairs of large size for $I\perp B$ is considerably higher than those for $I\|B$, naturally yielding different voltage drops. Comparing with the data in equilibrium, it is also clear that additional PVs are excited by external currents. Snapshots of real-space configurations of PV pairs in one CuO layer with size larger than 6 are shown in the insets of Fig. 5. By a careful inspection on the connection of these PVs with underlying JV lines, we find that all these large-sized pairs are associated with hops of JV segments, indicating clearly that the external magnetic field plays the crucial influence on dissipations. In the presence of the small external current, just those PV vortex pairs are broken first and yield the KT dynamical behavior for the high anisotropy case.

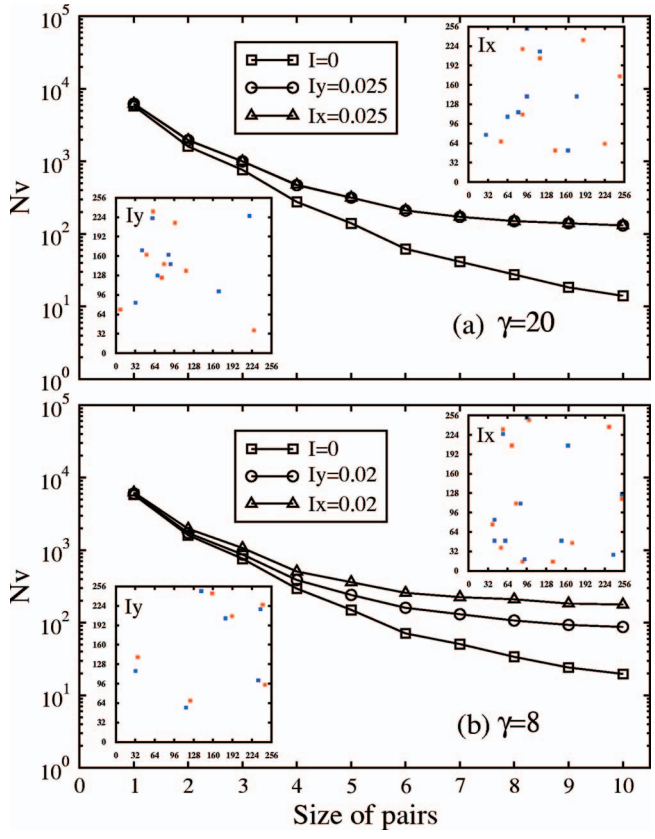

FIG. 5. (Color) Number of vortex pairs with size larger than the abscissa value at $T=0.9$ for (a) $\gamma=20$ and (b) $\gamma=8$. Insets show snapshots of vortices pair with sizes larger than 6 in one *ab* layer, with the upper one for $I\perp B$ and the low one for $I\|B$.

IV. CONCLUSIONS

A RSJ dynamics is introduced to the 3D frustrated anisotropic *XY* model, from which we can reveal both *microscopic* configurations of JVs and *macroscopic* voltages. The main conclusions are as follows: In the KT phase, an orientation-independent resistivity is found, which is caused by the meandering JV lines of QLR correlations. The *I-V* curves show a nice power-law behavior, and the *I-V* index jumps from 3 to 1 at the KT phase-transition point. In the 3D lattice phase, we find that the in-plane resistivity is orientation dependent for small currents. With the increase of currents, the orientational independent dispassion reappears.

ACKNOWLEDGMENTS

The present simulations were performed on the Numerical Materials Simulator (SX-5) at NIMS. This work was partially supported by National Natural Science Foundation of China under Grant No. 10574107, Program for New Century Excellent Talents in University in China, National Basic Research Program of China (Grant No. 2006CB601003) (Q.H.C.), by the Japan Society for the Promotion of Science [Grant-in-Aid for Scientific Research (C) Grant No. 18540360] and ITSNEM project, Chinese Academy of Science (X.H.).

[1] G. Blatter *et al.*, Rev. Mod. Phys. **66**, 1125 (1994); G. W. Crabtree and D. R. Nelson, Phys. Today **45**, 38 (1997).
[2] Y. Iye, S. Nakamura, and T. Tamegai, Physica C **159C**, 433 (1989).
[3] K. C. Woo, K. E. Gray, R. T. Kampwirth, J. H. Kang, S. J. Stein, R. East, and D. M. McKay, Phys. Rev. Lett. **63**, 1877 (1989).
[4] Y. Ando, N. Motohira, K. Kitazawa, J. I. Takeya, and S. Akita, Phys. Rev. Lett. **67**, 2737 (1991).
[5] A. K. Pradhan, S. J. Hazell, J. W. Hodby, C. Chen, Y. Hu, B. M. Wanklyn, Phys. Rev. B **47**, 11374 (1993).
[6] W. K. Kwok, V. Welp, G. W. Crabtree, K. G. Vandervoort, R. Hulscher, and J. Z. Liu, Phys. Rev. Lett. **64**, 966 (1990).
[7] S. Chakravarty, B. I. Ivlev, and Y. N. Ovchinnikov, Phys. Rev. Lett. **64**, 3187 (1990).
[8] G. Blatter, B. I. Ivlev, and J. Rhyner, Phys. Rev. Lett. **66**, 2392 (1991).
[9] V. L. Berezinsky, Sov. Phys. JETP **34**, 610 (1972).
[10] J. M. Kosterlitz and D. J. Thouless, J. Phys. C **6**, 1181 (1973).
[11] X. Hu and M. Tachiki, Phys. Rev. B **70**, 064506 (2004).
[12] X. Hu and M. Tachiki, Phys. Rev. Lett. **85**, 2577 (2000); **80**, 4044 (1998).
[13] X. Hu, M. Luo, and Y. Ma, Phys. Rev. B **72**, 174503 (2005).
[14] L. Golubovic and M. Golubovic, Phys. Rev. Lett. **80**, 4341 (1998); C. S. O'Hern and T. C. Lubensky, *ibid.* **80**, 4345 (1998).
[15] C. S. O'Hern, T. C. Lubensky, and J. Toner, Phys. Rev. Lett. **83**, 2745 (1999).
[16] S. L. Sondhi and K. Yang, Phys. Rev. B **63**, 054430 (2001).
[17] R. E. Hetzel, A. Sudbo, and D. A. Huse, Phys. Rev. Lett. **69**, 518 (1992); X. Hu, S. Miyashita, and M. Tachiki, *ibid.* **79**, 3498 (1997); P. Olsson and S. Teitel, *ibid.* **82**, 2183 (1999); A. E. Koshelev, Phys. Rev. B **56**, 11201 (1997).
[18] Q. H. Chen and X. Hu, Phys. Rev. Lett. **90**, 117005 (2003).
[19] B. J. Kim, P. Minnhagen, and P. Olsson, Phys. Rev. B **59**, 11506 (1999); D. Domínguez, Phys. Rev. Lett. **82**, 181 (1999).
[20] Q. H. Chen, L. H. Tang, and P. Tong, Phys. Rev. Lett. **87**, 067001 (2001); L. H. Tang and Q. H. Chen, Phys. Rev. B **67**, 024508 (2003).
[21] V. Ambegaokar, B. I. Halperin, D. R. Nelson, and E. D. Siggia, Phys. Rev. Lett. **40**, 783 (1978); Phys. Rev. B **21**, 1806 (1980).
[22] M. V. Simkin and J. M. Kosterlitz, Phys. Rev. B **55**, 11646 (1997).